Adsorption of thallium(I) on rutile nano-titanium dioxide and environmental implications

Juan Liu [1], **Weilong Zhang** [1], **Yang Wu** [1], **Haifeng Lu** [2], **Yongheng Chen** [1], **Jin Wang** Corresp., [1], **Shuijing Zhai** Corresp., [3], **Qiaohui Zhong** [1,4], **Wanying Zhong** [1], **Chunling Huang** [1], **Wenhui Zhang** [1], **Xiaoxiang Yu** [1], **Siyu Liu** [1]

[1] Innovation Center and Key Laboratory of Water Quality and Conservation in the Pearl River Delta, Ministry of Education, School of Environmental Science and Engineering, Guangzhou University, Guangzhou 510006, China

[2] Wuhan Digital Engineering Institute, Wuhan, 430205, China

[3] Key Laboratory of Humid Subtropical Eco-geographical Processes, Ministry of Education, College of Geography Science, Fujian Normal University, Fuzhou 350007, China

[4] Guangzhou Institute of Geochemistry, Chinese Academy of Sciences, Guangzhou 510405, China

Corresponding Authors: Jin Wang, Shuijing Zhai
Email address: wangjin@gzhu.edu.cn, S2008shuijing@163.com

Rutile nano-titanium dioxide (RNTD) characterized by loose particles with diameter in 20-50 nm has a very large surface area for adsorption of Tl, a typical trace metal that has severe toxicity. The increasing application of RNTD and widespread discharge of Tl-bearing effluents from various industrial activities would increase the risk of their co-exposure in aquatic environments. The adsorption behavior of Tl(I) (a prevalent form of Tl in nature) on RNTD was studied as a function of solution pH, temperature, and ion strength. Adsorption isotherms, kinetics, and thermodynamics for Tl(I) were also investigated. The adsorption of Tl(I) on RNTD started at very low pH values and increased abruptly, then maintained at high level with increasing pH > 9. Uptake of Tl(I) was very fast on RNTD in the first 15 min then slowed down. The adsorption of Tl(I) on RNTD was an exothermic process; and the adsorption isotherm of Tl(I) followed the Langmuir model, with the maximum adsorption amount of 51.2 mg/g at room temperature. The kinetics of Tl adsorption can be described by a pseudo-second-order equation. FT-IR spectroscopy revealed that -OH and -TiOO-H play an important role in the adsorption. All these results indicate that RNTD has a fast adsorption rate and excellent adsorption amount for Tl(I), which can thus alter the transport, bioavailability and fate of Tl(I) in aqueous environment.

1 Adsorption of thallium(I) on rutile nano-titanium dioxide and environmental implications

2 Juan Liu[1], Weilong Zhang[1], Yang Wu[1], Haifeng Lu[2], Yongheng Chen[1], Jin Wang[1*], Shuijing Zhai [3**], Qiaohui

3 Zhong[1, 4], Wanying Zhong[1], Chunling Huang[1], Wenhui Zhang[1], Xiaoxiang Yu[1], Siyu Liu[1]

4 1. Innovation Center and Key Laboratory of Water Quality and Conservation in the Pearl River Delta, Ministry

5   of Education, School of Environmental Science and Engineering, Guangzhou University, Guangzhou

6   510006, China.

7 2. Wuhan Digital Engineering Institute, Wuhan, 430205, China.

8 3. Key Laboratory of Humid Subtropical Eco-geographical Processes, Ministry of Education, College of

9   Geography Science, Fujian Normal University, Fuzhou 350007, China.

10 4. Guangzhou Institute of Geochemistry, Chinese Academy of Sciences, Guangzhou 510405, China.

12 **Abstract**

13 Rutile nano-titanium dioxide (RNTD) characterized by loose particles with diameter in 20-50 nm

14 has a very large surface area for adsorption of Tl, a typical trace metal that has severe toxicity.

15 The increasing application of RNTD and widespread discharge of Tl-bearing effluents from

16 various industrial activities would increase the risk of their co-exposure in aquatic environments.

17 The adsorption behavior of Tl(I) (a prevalent form of Tl in nature) on RNTD was studied as a

18 function of solution pH, temperature, and ion strength. Adsorption isotherms, kinetics, and

19 thermodynamics for Tl(I) were also investigated. The adsorption of Tl(I) on RNTD started at

20 very low pH values and increased abruptly, then maintained at high level with increasing pH > 9.

21 Uptake of Tl(I) was very fast on RNTD in the first 15 min then slowed down. The adsorption of

* Corresponding author.

E-mail addresses: wangjin@gzhu.edu.cn (J. Wang); S2008shuijing@163.com (S. Zhai).

22 Tl(I) on RNTD was an exothermic process; and the adsorption isotherm of Tl(I) followed the

23 Langmuir model, with the maximum adsorption amount of 51.2 mg/g at room temperature. The

24 kinetics of Tl adsorption can be described by a pseudo-second-order equation. FT-IR

25 spectroscopy revealed that -OH and -TiOO-H play an important role in the adsorption. All these

26 results indicate that RNTD has a fast adsorption rate and excellent adsorption amount for Tl(I),

27 which can thus alter the transport, bioavailability and fate of Tl(I) in aqueous environment.

28 **Keywords:** thallium; adsorption behavior; rutile nano-titanium dioxide

1. Introduction

Thallium is a heavy metal whose toxicity to mammals is second only to that of methylmercury and far exceeds that of chromium, mercury, and lead (Campanella et al., 2016; Campanella et al., 2017; Casiot et al., 2011; Galván-Arzate & Santamaría, 1998; Grösslová et al., 2018; Li et al., 2012; Liu et al., 2016a; Perotti et al., 2017). Thallium can be accumulated in bone marrow, kidneys and different organs, thereby affecting the gastrointestinal and urinary tract, and even causing permanent damage in muscle atrophy or central nervous system (Galván-Arzate & Santamaría, 1998; Peter & Viraraghavan, 2005). Hence, Tl was listed as one of the toxic pollutants of priority both in USA and China (Xiao et al., 2012).

Thallium pollution is mainly due to widespread use of Tl-containing minerals in industry. For example, mining of Hg-As-Tl deposits at Lanmuchang in Guizhou, southwestern China, led to severe Tl poisoning in local residents during the 1960–1970s (Xiao et al., 2004a; Xiao et al., 2004b; Xiao et al., 2004c; Xiao et al., 2007; Xiao et al., 2012). Waste discharge from a Pb-Zn smelter using Tl-bearing minerals resulted in Tl pollution in the Northern Branch of the Pearl River in 2010 (Liu et al., 2016b; Liu et al., 2017).

In recent years, rutile nano-titanium dioxide (RNTD) have been widely employed in a variety of products (*eg*. paints, cosmetics, optical component, biosensors and sunscreen) (Kusior et al., 2017). The rapid growth in TiO_2 production and its industrial applications may result in enhanced release into the environment and exposure to human (Danielsson et al., 2018; Liu, 2005). Having large surface area, TiO_2 nano-particles can alter the transport, bioavailability and fate of heavy metals by strong adsorption interactions. It is likely for Tl(I) and RNTD to encounter and co-exist in the aqueous environment. The adsorption of various heavy metals (such as Pb, Zn, Cd and Cu) on RNTD has been extensively investigated, but it remains unclear for the adsorption behavior of Tl on RNTD (Jiang et al., 2014).

In this study, batch experiments were conducted to explore the adsorption behavior of Tl on

55 RNTD. The effects of various parameters—RNTD dosage, ionic strength, pH, time, initial

56 concentration of Tl, and temperature—on the adsorption behavior, as well as the adsorption

57 isotherms, kinetics, and thermodynamics of Tl(I), were investigated.

58 **2. Materials and methods**

59 **2.1 Materials**

60 Analytical reagent (AR)-grade RNTD was purchased from Aladdin Reagents Co., Ltd. (Shanghai,

61 China). Thallium(I) nitrate (99.5%, metal basis) was purchased from Alfa Aesar, A Johnson

62 Matthey Company. AR-grade $NaClO_4$, $HClO_4$, and NaOH were obtained from Guangzhou

63 Chemical Reagent Co., Ltd. (China). All experiments were performed using Milli-Q water

64 (Millipore Corp.).

65 **2.2 Batch adsorption experiments**

66 All the batch adsorption experiments were conducted in a rotary shaker (25 ± 0.2 °C, 200 rpm)

67 using a 50 mL PP centrifuge tube. The pH was adjusted to the desired value by using 0.1 mol/L

68 $HClO_4$ or NaOH. Stock solution of $TlNO_3$ (100 mg/L) was prepared with deionized water.

69 First, the influence of RNTD dosage on the adsorption of Tl(I) was studied. For this purpose, the

70 concentration of RNTD was set in the range 0.5 to 5 g/L at desired intervals, using 0.1 mol/L

71 $NaClO_4$ as the background, to ensure constant ionic strength with pH 7.0 ± 0.3. To investigate

72 the effect of ionic strength on Tl(I) adsorption, an appropriate amount of $NaClO_4$ was added with

73 the concentration ranging from 0.05 to 3 mol/L at desired intervals. The influence of pH on Tl(I)

74 adsorption was studied in the range of 2 to 11. For isotherm studies, the temperature was set at

75 298 K, 303 K and 313 K, respectively, and the initial concentration of Tl(I) varied from 0.02 to

76 20 mg/L. The solutions obtained were filtered rapidly through a 0.45 mm membrane after 300

77 min, and Tl concentration was measured immediately by adsorption thermodynamics

78 experiments. To evaluate the adsorption kinetics, samples were collected at desired intervals in

79   the range of 0 to 300 min. The concentration of Tl(I) was determined by inductively coupled

80   plasma–mass spectrometry (ICP-MS; NexION, PerkinElmer US).

81   The adsorption amount and adsorption rate are calculated as follows:

82    $$\text{Adsorption rate:} \alpha\% = \frac{C_0 - C_s}{C_0} \times 100\% \qquad (1)$$

83    $$\text{Adsorption amount:} Q_e = \frac{(C_0 - C_s)V}{m} \qquad (2)$$

84   Where, C_0 - initial concentration (mg/L);

85   C_s - remaining concentration of Tl after adsorption (mg/L);

86   V - solution volume (L);

87   m -total mass of adsorbent added (g).

88   **2.3 Characterization**

89   The morphologies of RNTD were observed by a JSM-7001F scanning electron microscopy

90   (SEM, JOEL, Japan) integrated with an energy-dispersive X-ray spectrometer (Oxford

91   Instruments, UK). To examine surface properties, FTIR absorption spectra of TiO_2 nanomaterials

92   were analyzed by using a Bruker (TENSOR27, Germany) FTIR spectrometer in the frequency

93   range of 400–4000 cm^{-1}, operating with a spectral resolution of 2 cm^{-1}. The crystal phase of the

94   sample was visualized by X-ray powder diffraction (XRD) using an X'Pert Pro Diffractometer

95   (PANanalytical, The Netherlands) X-ray diffractometry operating at 100 kV and 40 mA, using

96   Cu Ka radiation at a scan speed of 4°/min.

97   **3.   Results and discussion**

98   **3.1 Effect of RNTD dosage**

99   The adsorption effect of adsorbent on Tl is due to the existence of active adsorption sites in the

100   adsorbent. Under a constant initial Tl concentration, increase of the dosage of adsorbent will

101 enhance the contact site, thereby increasing the adsorption amount of adsorbent on Tl (Shen et al.,

102 2009). However, a decrease in adsorption amount with increased dosage was observed (Fig. 1),

103 and the adsorption rate increased from 55.4% to 92% as the dosage increased from 0.5 to 2.5 g/L.

104 It did not continue to rise afterwards due to further addition of the adsorbent will cause difficulty

105 in dispersion, which can hinder Tl adsorption. According to the literature, the mass of TiO_2

106 particles could increase the sedimentation aggregation (He & Zhang, 2003).

3.2 Effect of initial thallium concentration

108 Initial concentration of Tl in natural systems will also influence Tl adsorption behavior (Zhang et

109 al., 2017). As shown in Fig. 2, at 0.02 to 10 mg/L, as the initial concentration increases, the

110 adsorption rate shows a tendency to decrease unevenly from 70%. From 10 to 20 mg/L, the

111 adsorption rate no obvious change with the initial concentration. Obviously, without changing

112 the amount of adsorbent, if initial Tl concentration in the water is higher, the nano TiO_2 can

113 adsorb more Tl. The adsorption rate no longer decreases at initial Tl concentration of 10 mg/L.

114 From the perspective of cost savings, the Tl concentration of 10 mg/L would be most suitable for

115 adsorption by rutile nano TiO_2, which deserves highest environmental benefits.

3.3 Effect of ionic strength

117 Another important factor affecting Tl(I) concentration in natural systems is ionic strength (Liu et

118 al., 2011). As shown in Fig. 3, with an increase of $NaClO_4$ concentration, the adsorption rate

119 gradually increased from 33.6% to 86.7% and then tended to reach equilibrium. The adsorption

120 of Tl mainly depends on the surface negative charge of the adsorbent. Increasing $NaClO_4$

121 concentration is favorable for adsorption, but excessive concentrations reduce adsorption rate.

122 When $NaClO_4$ concentration is > 1.5 mol/L, the adsorption rate tends to become constant (Vilar

123 et al., 2005). At this time, the adsorption increases with the increase of the ionic strength or is not

124 sensitive to the ion concentration. It is likely that the inner surface complex (ISSC) is formed

125 between RNTD and Tl, the chemical bond between RNTD and Tl is generally a coordination

126 covalent bond.

3.4 Effect of pH

The effect of the pH value of the solution on the adsorption is mainly achieved by changing the charge carried by the adsorbent and the adsorbate, thereby affecting the electrostatic interaction between the adsorbent and the adsorbate (Wu et al., 2005; Wu et al., 2004). As shown in Fig. 4, the pH of the solution exerted a significant role on the adsorption of Tl(I). The adsorption percentage rised from 28.9% to 60.2% when the pH increased from 2 to 11. No obvious change in the adsorption occurred from pH 2 to pH 5. The adsorption amount increased slowly in the pH range from 2 to 5, but very significantly in the pH range from 5 to 9, followed by a plateau at pH 9 to 11. In aqueous solution, Tl^+ is the predominant species in the pH range of 2–11. The elevated adsorption amount with pH can be owing to pH_{pzc} of the RNTD adsorbent (Govender et al., 2007; Mahamuni et al., 1999; Vayssieres et al., 2001). At pH values of 2~5, which are lower than pH_{pzc}, the surface charge of the RNTD was positive. It facilitated great electrostatic repulsion between Tl^+ and positively-charged RNTD, which inhibited adsorption of Tl(I) ions. At pH values (6~9) higher than pH_{pzc}, the surface charge of the TNTs turned negative, which promoted the adsorption of Tl^+, due to the electrostatic force of attraction between Tl(I) ions and the surface. For further increase in pH, approximately 60% removal efficiency was achieved when pH was above 9, suggesting a fairy good adsorption performance of RNTD.

3.5 Adsorption kinetics

As shown in Fig. 5, the adsorption amount rapidly increased from 2.8 to 3.3 mg/g in the first 5-15 min but did not change significantly further on, indicating a rapid adsorption of Tl(I) by RNTD. The adsorption process was complete within 15 min, The rapid uptake was mainly due to the large amount of active sites on the surface of the RNTD.

In order to better understand the behavior of Tl(I) adsorption and possible controlling mechanism, the kinetics experimental data were fitted with the commonly used kinetic models, such as pseudo first-order, pseudo second-order, and Elovich models (Liu et al., 2014; Pu et al., 2013).

Pseudo-first-order kinetic model equation is expressed by:

153
$$\lg(Q_e - Q_t) = \lg Q_e - (k_1 t)/2.303 \qquad (3)$$

154 Where Q_e is the adsorption amount (mg/g); Q_t is the adsorption amount (mg/g) at time t; and k_1 is

155 the first-order adsorption rate constant (g/mg•min).

156 Pseudo-second-order kinetic model equation is expressed as follows:

157
$$t/Q_t = 1/k_2 Q_e^2 + t/Q_e \qquad (4)$$

158 Where Q_e is the adsorption amount (mg/g); Q_t is the adsorption amount (mg/g); k_2 is the

159 secondary adsorption rate constant (g/mg•min).

160 Elovich dynamic model is expressed by:

161
$$Q_t = k_e \times \ln t + C \qquad (5)$$

162 Where Q_t is the adsorption amount (mg/g) at time t; k_e and C are constants; t is the adsorption

163 time (min); and k_e is related to the adsorption efficiency. The greater the k_e value, the higher is

164 the adsorption efficiency.

165 As listed in Table 1, the kinetic results are fitted by the pseudo-second-order model very well,

166 with a high correlation coefficient (R^2= 0.9969). This suggests that the rate-controlling step for

167 the adsorption was the initial diffusion of metal ions from the solution and their subsequent

168 interaction with the -ONa/-OH groups on the RNTD surface, and the subsequent interaction

169 between the -ONa/-OH groups of RNTD and the metal ions.

170 **3.6 Adsorption isotherms**

171 With an increase in the initial Tl(I) concentration, the adsorption rate showed a trend of decrease

172 from 70% to 50% (Fig. 6). The lowest adsorption amount was found at the reaction temperature

173 of 313 K, while higher adsorption amounts were observed at   lower temperatures, which

174 indicates that the adsorption is exothermic. The adsorption amount of RNTD showed a near-

175 linear dependent on the initial Tl concentration. The adsorption of Tl(I) was reduced by increase

176 of temperature. Differences between adsorption isotherm become smaller at higher temperature.

177 Langmuir and Freundlich adsorption models were used to fit the experimental data of Tl(I).

178 The equation for the Langmuir adsorption model is

179
$$C_e/Q_e = C_e/Q_{max} + 1/(Q_{max} \times b)$$
(6)

180 Where Q_e is the adsorption amount (mg/g); Q_{max} is the maximum adsorption amount (mg/g); C_e

181 is Tl concentration at adsorption equilibrium (mg/L); and b is the adsorption equilibrium

182 constant (L/mg).

183 The equation for the Freundlich adsorption model is

184
$$\ln Q_e = \ln k + (1/n)\ln C_e$$
(7)

185 Where Q_e is the adsorption amount (mg/g); k and n are constants; and C_e is Tl concentration at

186 adsorption equilibrium (mg/L);

3.7 Adsorption thermodynamics

188 The thermodynamic parameters provide in-depth information about the inherent energetic

189 changes associated with adsorption. The standard enthalpy change (ΔH^o), standard entropy

190 change (ΔS^o), and Gibbs free energy change (ΔG^o) can be calculated from the temperature-

191 dependent adsorption data using the following equations:

192
$$\Delta G = RT\ln K_s$$
(8)

193
$$\Delta G = \Delta H - T\Delta S$$
(9)

194
$$\ln K_s = -\frac{\Delta H}{RT} + \frac{\Delta S}{R}$$
(10)

195 where R is the gas constant; K_s is the equilibrium constant; and T is the absolute temperature.

196   ΔH^o and ΔS^o were obtained from the slope and intercept of the linear plot of $\ln K_s$ versus $1/T$,

197   respectively. The thermodynamic parameters calculated from Eqs. (5) to (7) are summarized in

198   Table 2. The results showed that the adsorption amount of Tl(I) decreased with increasing

199   temperature. The negative values of ΔH^o indicated that the adsorption of Tl was exothermic. This

200   can be explained by the fact that the heat of adsorption of Tl(I) on RNTD exceeds the

201   dehydration energy of the Tl(I) ions during adsorption. The negative values of ΔS^o showed that

202   adsorption of Tl decreased the randomness of the liquid–solid system. The negative values of

203   ΔG^o suggested that the adsorption of Tl was spontaneous.

204   **4. Characterization of Tl adsorption**

205   **4.1 FTIR analysis**

206   Fig. 7 exhibited the FTIR spectra of pure RNTD and RNTD after Tl adsorption. The peaks at
207   ~1045 cm^{-1} and the strong signal between 2600~3600 cm^{-1} were ascribed to hydroxyl bond O－H

208   stretching (water adsorbed on TiO_2) (Tanzifi et al., 2018). The wide peak between 600 and 800
209   cm^{-1} corresponded to Ti－O－Ti bonds was observed at both of the spectra. The weak absorption

210   peak at ~2360 cm^{-1} corresponds to the stretching vibration of TiOO-H. A strong peak attributed

211   to ClO_4^- is seen at 1085.8 cm^{-1}. It can be due to the ion exchange between ClO_4^- on the surface of

212   the RNTD after addition of $NaClO_4$. A vibration peak due to physically adsorbed water appears

213   at 1637.5 cm^{-1} (Yousefzadeh et al., 2018).

214   **4.2 SEM and XRD analyses**

215   As shown in the SEM images (Fig. 8), the surface of TiO_2 nano-particles before adsorption was

216   covered by loose particles with diameter in nm, which implies a large specific surface area. After

217   adsorption, due to the hydrophilicity of TiO_2, ultrafine nanoparticles moved randomly in the

218   aqueous phase, diffused, and spontaneously agglomerated to produce secondary particle

219   clumping. Thus, a dispersed system of micron-sized and nano-sized TiO_2 coexists in the solution,

220   between the colloidal system and the coarsely dispersed system (Fig. 8).

221 The XRD patterns of pure RNTD and RNTD after Tl adsorption were presented in Fig. 9. Not

222 obvious differences were observed between the two patterns. Anatase and rutile phases of

223 TiO_2 were observed in both of the patterns at the 2θ angles of 27.48、36.12、39.24、41.28、

224 44.08、54.36、56.68、62.80、64.12、69.04、69.80°. It matched well with the standard data

225 for TiO_2 diffraction pattern (JCPDS89-4920) (Maleki et al., 2016).

226 **5. Environmental implications**

227 As shown in the study, RNTD has a fast adsorption rate and excellent adsorption amount for

228 Tl(I). It is possible that Tl(I) would release from RNTD when ingested by organisms, which may

229 greatly increases the risk of Tl to the environment and organisms. In addition, RNTD may be

230 modified differently in the environment, complicating the interaction between Tl(I) and RNTD.

231 Moreover, the prevalence of organic matter and other heavy metal ions in aqueous environments

232 may also contribute to the dispersion and adsorption of Tl(I) on RNTD.

233 **6. Conclusion**

234 The results showed that the Tl(I) adsorption amount of nano-TiO_2 increased with increasing pH.

235 Efficient adsorption of Tl(I) was found to occur even at a pH as low as 2, whereas the optimum

236 pH for Tl(I) adsorption was approximately 9–10. The adsorption was rapid, with high removal

237 efficiency of Tl (I) more than 40% in the first 15 min. The adsorption of Tl(I) on nano-TiO_2

238 fitted well to the Langmuir isotherm, with a calculated maximum adsorption amount of 51.2

239 mg/g at room temperature, indicating monolayer adsorption sites for Tl on the adsorbent surface.

240 The adsoprtion was found to be an exothermic process. The pseudo-second-order equation could

241 best fit the kinetics of Tl adsorption (R^2=0.9969). All these results suggest the pivotal role of

242 RNTD on altering the transport, bioavailability and fate of Tl(I) in aqueous environment. More

243 works are necessary to improve the understanding of the transport and fate of nano-titanium

244 dioxide and Tl(I).

245

246 **References**

247 **Véronique Adam, Stéphanie Loyaux-Lawniczak, & Quaranta G. 2015.** Characterization of engineered Tio$_2$
248   nanomaterials in a life cycle and risk assessments perspective. *Environmental Science and Pollution*
249   *Research.* **22**(15):11175-92 DOI 10.1007/s11356-015-4661-x.

250 **Campanella B, Casiot C, Onor M, Perotti M, Petrini R, and Bramanti E. 2017.** Thallium release from acid mine
251   drainages: Speciation in river and tap water from Valdicastello mining district (northwest Tuscany).
252   *Talanta* **171**:255-261 DOI 10.1016/j.talanta.2017.05.009.

253 **Campanella B, Onor M, D'Ulivo A, Giannecchini R, D'Orazio M, Petrini R, and Bramanti E. 2016.** Human exposure
254   to thallium through tap water: A study from Valdicastello Carducci and Pietrasanta (northern Tuscany,
255   Italy). *Science of the Total Environment* **548-549**:33-42 DOI 10.1016/j.scitotenv.2016.01.010.

256 **Casiot C, Egal M, Bruneel O, Verma N, Parmentier M, and Elbazpoulichet F. 2011.** Response to Comment on
257   "Predominance of Aqueous Tl(I) Species in the River System Downstream from the Abandoned Carnoulès
258   Mine (Southern France)". *Environmental Science & Technology* **45**:2056-2064 DOI 10.1021/es204479k.

259 **Danielsson K, Persson P, Gallego-Urrea JA, Abbas Z, Rosenqvist J, and Jonsson CM. 2018.** Effects of the
260   adsorption of NOM model molecules on the aggregation of TiO$_2$ nanoparticles in aqueous
261   suspensions. *Nanoimpact* **10**:177-187 DOI 10.1016/j.impact.2018.05.002.

262 **Galván-Arzate S, and Santamaría A. 1998.** Thallium toxicity. *Toxicol Lett* **99**:1-13 DOI 10.1016/S0378-
263   4274(98)00126-X.

264 **Govender K, Boyle DS, O'Brien P, Binks D, West D, and Coleman D. 2007.** Room-Temperature Lasing
265   Observed from ZnO Nanocolumns Grown by Aqueous Solution Deposition. *Aiche Meeting* DOI
266   10.1002/chin.200247008.

267 **Grösslová Z, Vaněk A, Oborná V, Mihaljevič M, Ettler V, Trubač J, Drahota P, Penížek V, Pavlů L, and Sracek
268   O. 2018.** Thallium contamination of desert soil in Namibia: Chemical, mineralogical and isotopic
269   insights. *Environmental Pollution* **239**:272-280 DOI 10.1016/j.envpol.2018.04.006.

270 **He W, and Zhang XD. 2003.** Study of the reunion control of nanocrystalline TiO$_2$. *Rare Metal Materials &*
271   *Engineering* **32**:816-819

272 **Kusior A, Banas J, Trenczek-Zajac A, Zubrzycka P, Micek-Ilnicka A, and Radecka M. 2017.** Structural
273   properties of TiO$_2$ nanomaterials. *Journal of Molecular Structure* 1157 DOI
274   10.1016/j.molstruc.2017.12.064.

275 **Li S, Xiao TF, and Zheng B. 2012.** Medical geology of arsenic, selenium and thallium in China. *Science of the*
276   *Total Environment* **421-422**:31 DOI 10.1016/j.scitotenv.2011.02.040.

277 **Liu C. 2005.** Effect of Nano-TiO$_2$ on Strength of Naturally Aged Seeds and Growth of Spinach. *Biological Trace*
278   *Element Research* **104**:83-91 DOI 10.1385/bter:104:1:083.

279 **Liu J, Luo X, Wang J, Xiao TF, Chen D, Sheng G, Yin ML, Lippold H, Wang C, and Chen Y. 2017.** Thallium
280   contamination in arable soils and vegetables around a steel plant-A newly-found significant source of
281   Tl pollution in South China. *Environmental Pollution* **224**:445-453 DOI 10.1016/j.envpol.2017.02.025.

282 **Liu J, Wang J, Chen YH, Xie X, Qi J, Lippold H, Luo D, Wang C, Su L, and He L. 2016a.** Thallium transformation
283   and partitioning during Pb-Zn smelting and environmental implications. *Environmental Pollution*
284   **212**:77 DOI 10.1016/j.envpol.2016.01.046.

285 **Liu J, Wang J, Chen YH, Xie X, Qi J, Lippold H, Luo D, Wang C, Su L, and He L. 2016b.** Thallium transformation
286   and partitioning during Pb–Zn smelting and environmental implications. *Environmental Pollution*
287   **212**:77-89 DOI 10.1016/j.envpol.2016.01.046.
288 **Liu J, Lippold H, Wang J, Lippmann-Pipke J, and Chen YH. 2011.** Sorption of thallium(I) onto geological
289   materials: Influence of pH and humic matter. *Chemosphere* **82:** 866-871 DOI
290   10.1016/j.chemosphere.2010.10.089.
291 **Liu W, Zhang P, Alistair GLB, Chen H, and Ni JR. 2014.** Adsorption mechanisms of thallium(I) and thallium(III)
292   by titanate nanotubes: Ion-exchange and co-precipitation. *Journal of Colloid and Interface Science*
293   **423:** 67-75 DOI 10.1016/j.scitotenv.2011.04.008.
294 **Mahamuni S, Borgohain K, Bendre BS, Leppert VJ, and Risbud SH. 1999.** Spectroscopic and structural
295   characterization of electrochemically grown ZnO quantum dots. *Journal of Applied Physics* **85**:2861-
296   2865 DOI 10.1063/1.369049.
297 **Maleki A, Hayati B, Najafi F, Gharibi F, and Sang WJ. 2016.** Heavy metal adsorption from industrial
298   wastewater by PAMAM/TiO_2 nanohybrid: Preparation, characterization and adsorption studies.
299   *Journal of Molecular Liquids* **224**:95-104 DOI 10.1016/j.molliq.2016.09.060.
300 **Perotti M, Petrini R, D'Orazio M, Ghezzi L, Giannecchini R, and Vezzoni S. 2017.** Thallium and Other
301   Potentially Toxic Elements in the Baccatoio Stream Catchment (Northern Tuscany, Italy) Receiving
302   Drainages from Abandoned Mines. *Mine Water & the Environment* 1-11 DOI 10.1007/s10230-017-
303   0485-x.
304 **Peter ALJ, and Viraraghavan T. 2005.** Thallium: a review of public health and environmental concerns.
305   *Environment International* **31**:493-501 DOI 10.1016/j.envint.2004.09.003.
306 **Pu YB, Yang XF, Zheng H, Wang DS, Su Y, and He J. 2013.** Adsorption and desorption of thallium(I) on
307   multiwalled carbon nanotubes. *Chemical Engineering Journal* **219:** 403-410 DOI
308   https://doi.org/10.1016/j.cej.2013.01.025.
309 **Shen YF, Tang J, Nie ZH, Wang YD, Ren Y, and Zuo L. 2009.** Preparation and application of magnetic Fe_3O_4
310   nanoparticles for wastewater purification. *Separation & Purification Technology* **68**:312-319 DOI
311   10.1016/j.seppur.2009.05.020.
312 **Tanzifi M, Yaraki MT, Karami M, Karimi S, Kiadehi AD, Karimipour K, and Wang S. 2018.** Modelling of dye
313   adsorption from aqueous solution on polyaniline/carboxymethyl cellulose/TiO_2 nanocomposites.
314   *Journal of Colloid & Interface Science* **519**:127-133 DOI 10.1016/j.jcis.2018.02.059.
315 **Vayssieres L, Keis K, Steneric Lindquist A, and Hagfeldt A. 2001.** Purpose-Built Anisotropic Metal Oxide
316   Material: 3D Highly Oriented Microrod Array of ZnO. *Journal of Physical Chemistry B* **105**:3350-3352
317   DOI 10.1021/jp010026s.
318 **Vilar VJP, Botelho CMS, and Rui ARB. 2005.** Influence of pH, ionic strength and temperature on lead
319   biosorption by Gelidium and agar extraction algal waste. *Process Biochemistry* **40**:3267-3275 DOI
320   10.1016/j.procbio.2005.03.023.
321 **Wu Z, Joo H, and Lee K. 2005.** Kinetics and thermodynamics of the organic dye adsorption on the
322   mesoporous hybrid xerogel. *Chemical Engineering Journal* **112**:227-236 DOI
323   10.1016/j.cej.2005.07.011.

324 **Xiao TF, Guha J, Boyle D, Liu CQ, Zheng B, Wilson GC, Rouleau A, and Chen J. 2004a.** Naturally occurring
325   thallium: a hidden geoenvironmental health hazard? *Environment International* **30:**501-507 DOI
326   10.1016/j.envint.2003.10.004.
327 **Xiao TF, Guha J, Dan B, Liu CQ, and Chen J. 2004b.** Environmental concerns related to high thallium levels in
328   soils and thallium uptake by plants in southwest Guizhou, China. *Science of the Total Environment*
329   318:223 DOI 10.1016/S0048-9697(03)00448-0.
330 **Xiao TF, Guha J, Liu CQ, Zheng B, Wilson G, Ning Z, and He L. 2007.** Potential health risk in areas of high
331   natural concentrations of thallium and importance of urine screening. *Applied Geochemistry* **22**:919-
332   929 DOI 10.1016/j.apgeochem.2007.02.008.
333 **Xiao TF, Yang F, Li S, Zheng B, and Ning Z. 2012.** Thallium pollution in China: A geo-environmental
334   perspective. *Science of the Total Environment* **421-422**:51-58 DOI 10.1016/j.scitotenv.2011.04.008.
335 **Xiao TF, Guha J, and Boyle D. 2004c.** High Thallium Content in Rocks Associated with Au-As-Hg-Tl and Coal
336   Mineralization and Its Adverse Environmental Potential in SW Guizhou, China. *Geochemistry-*
337   *exploration Environment Analysis* **4**:243-252 DOI 10.1144/1467-7873/04-204.
338 **Yousefzadeh H, Salarian AA, and Kalal HS. 2018.** Study of Pb (II) adsorption from aqueous solutions by TiO_2
339   functionalized with hydroxide ethyl aniline (PHEA/n-TiO_2). *Journal of Molecular Liquids* DOI
340   10.1016/j.molliq.2018.03.023.
341 **Wu ZJ, Ik-SungAhn, Lin YX, Huang LY, Lan XR, and KangtaekLee. 2004.** Methyl orange adsorption by
342   microporous and mesoporous TiO_2-SiO_2 and TiO_2-SiO_2-Al_2O_3 composite xerogels. *Composite*
343   *Interfaces* **11**:205-212 DOI 10.1163/156855404322971459.
344 **Zhang GS, Fan F, Li XP, Qi JY, and Chen YH. 2017.** Superior adsorption of thallium(I) on titanium peroxide: performance
345   and mechanism. *Chemical Engineering Journal* **331:** 471-479 DOI 10.1016/j.cej.2017.08.053.
346

347

348

349

350

351

352

353

354

355

356

357

358   **Table captions**

359   Table 1. Kinetic parameters for adsorption of Tl(I) on rutile nano-TiO_2

360   Table 2. Isotherm parameters for adsorption of Tl(I) on rutile nano-TiO_2

361

362   **Figure captions**

363   Fig. 1. Effect of rutile nano-TiO_2 dosage on Tl adsorption

364   Fig. 2. Effect of initial concentration on adsorption of Tl by rutile nano-TiO_2

365   Fig. 3. Effect of ionic strength on adsorption of Tl by rutile nano-TiO_2

366   Fig. 4. Effect of pH on adsorption of Tl by rutile nano-TiO_2

367   Fig. 5. Effect of time on adsorption of Tl by rutile nano-TiO_2

368   Fig. 6. Adsorption isotherms of Tl on rutile nano-TiO_2

369   Fig. 7. Infrared spectra of rutile nano-TiO_2

370   Fig. 8. SEM images of rutile nano-TiO_2: (a) before adsorption; (b) after adsorption

371   Fig. 9. X-ray diffraction pattern of rutile nano-TiO_2; (a) Before adsorption; (b) After adsorption

Figure 1

Effect of rutile nano-TiO$_2$ dosage on Tl adsorption
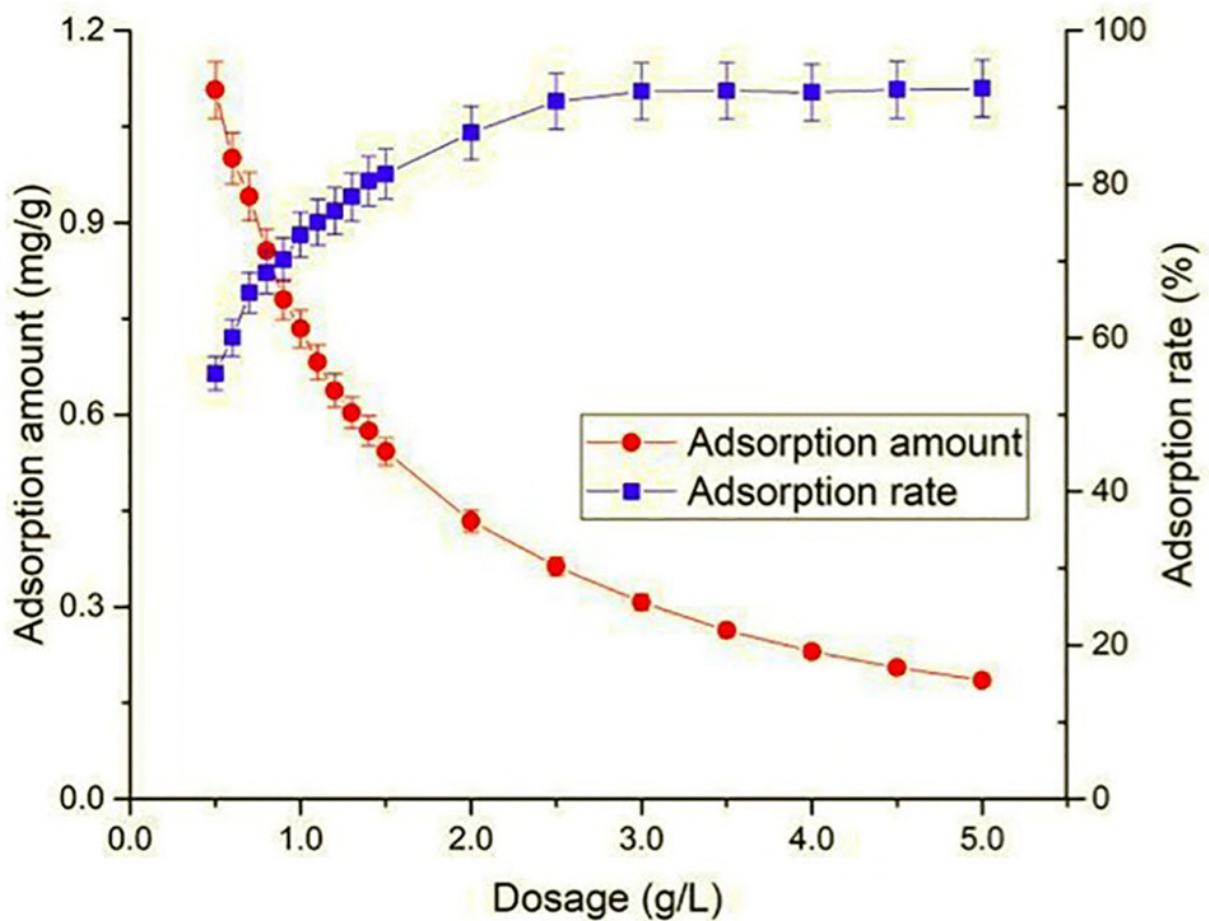
Figure 2

Effect of initial concentration on adsorption of Tl by rutile nano-TiO$_2$
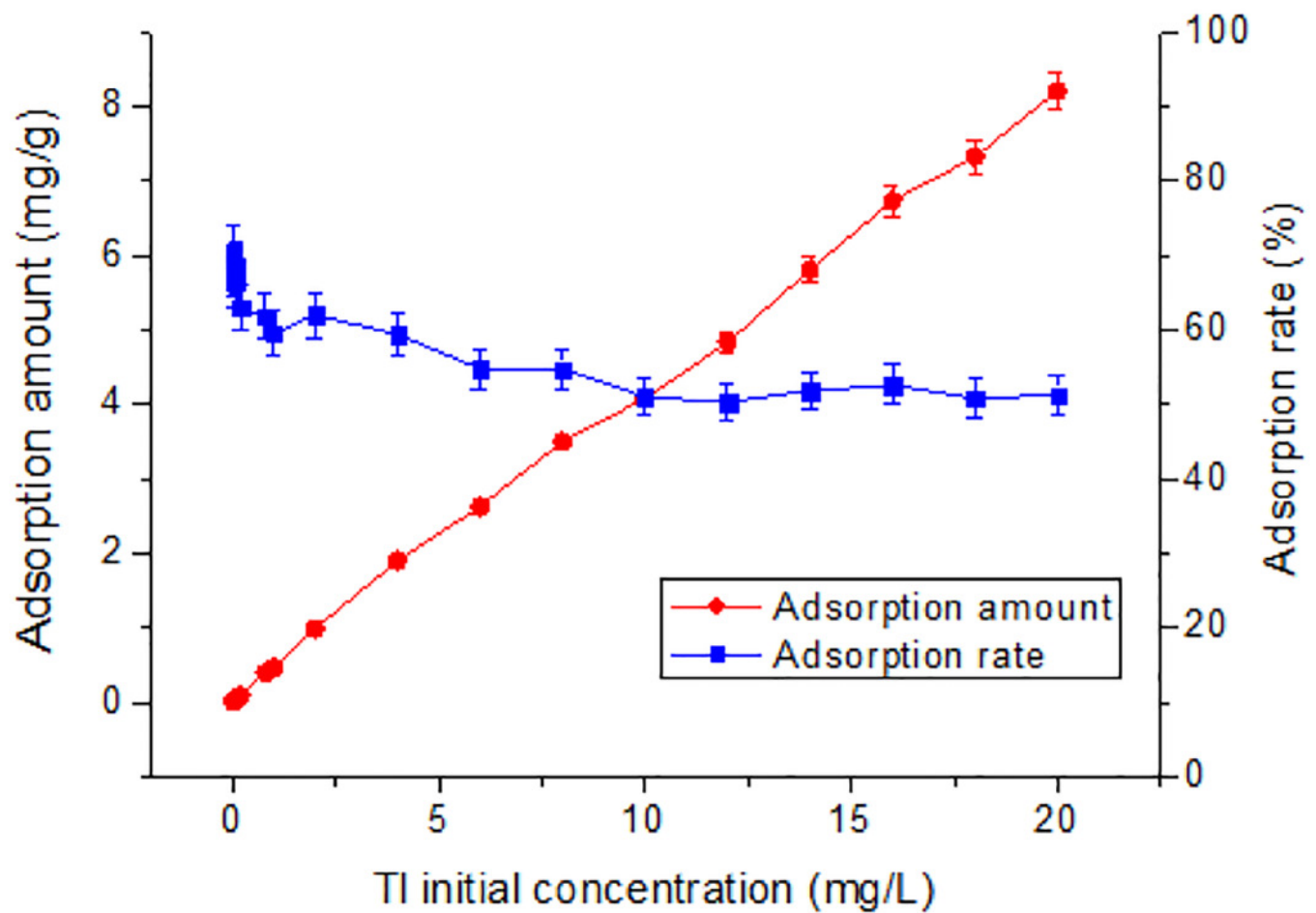
Figure 3

Effect of ionic strength on adsorption of Tl by rutile nano-TiO$_2$
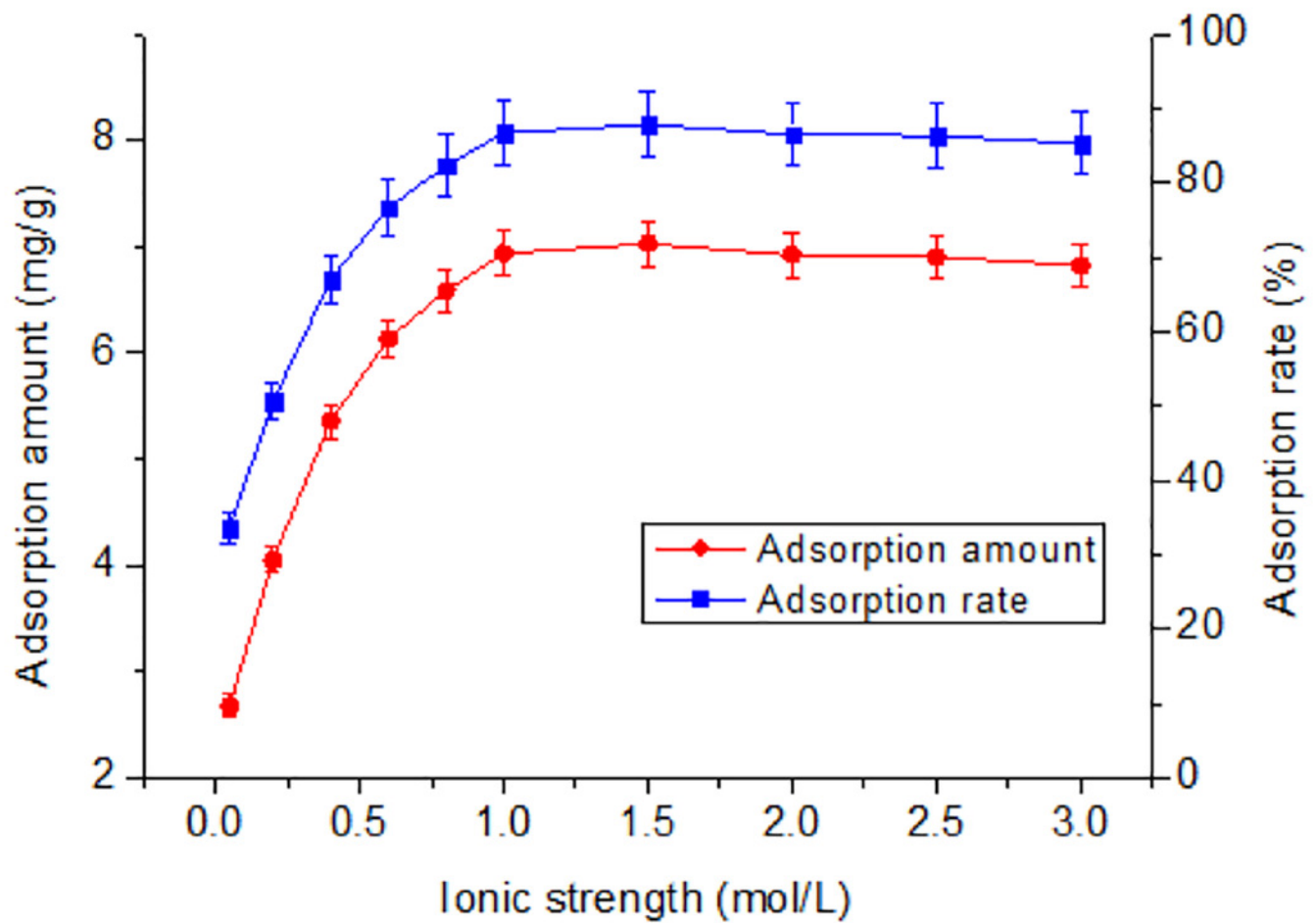
Figure 4

Effect of pH on adsorption of Tl by rutile nano-TiO$_2$
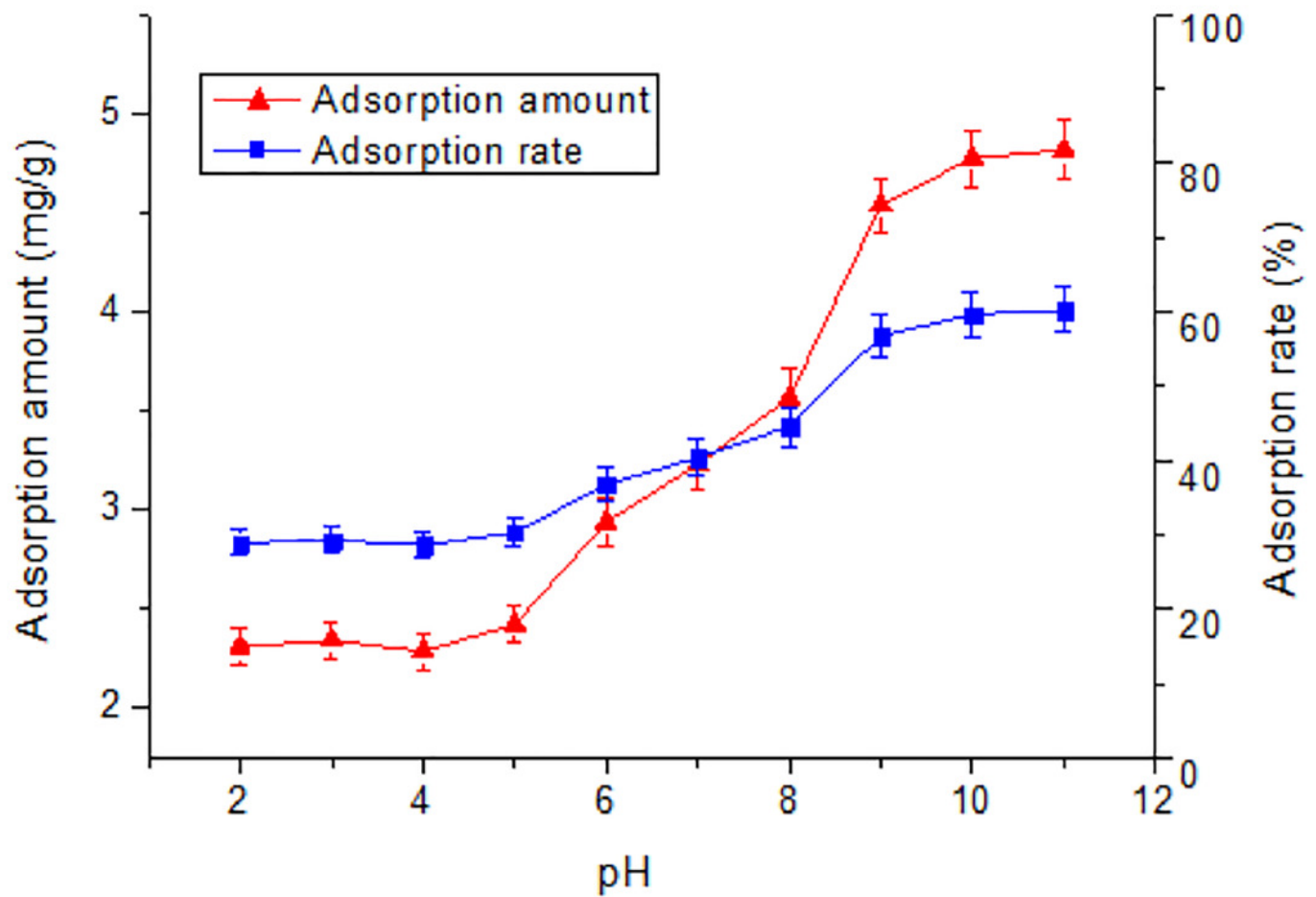
Figure 5

Effect of time on adsorption of Tl by rutile nano-TiO$_2$
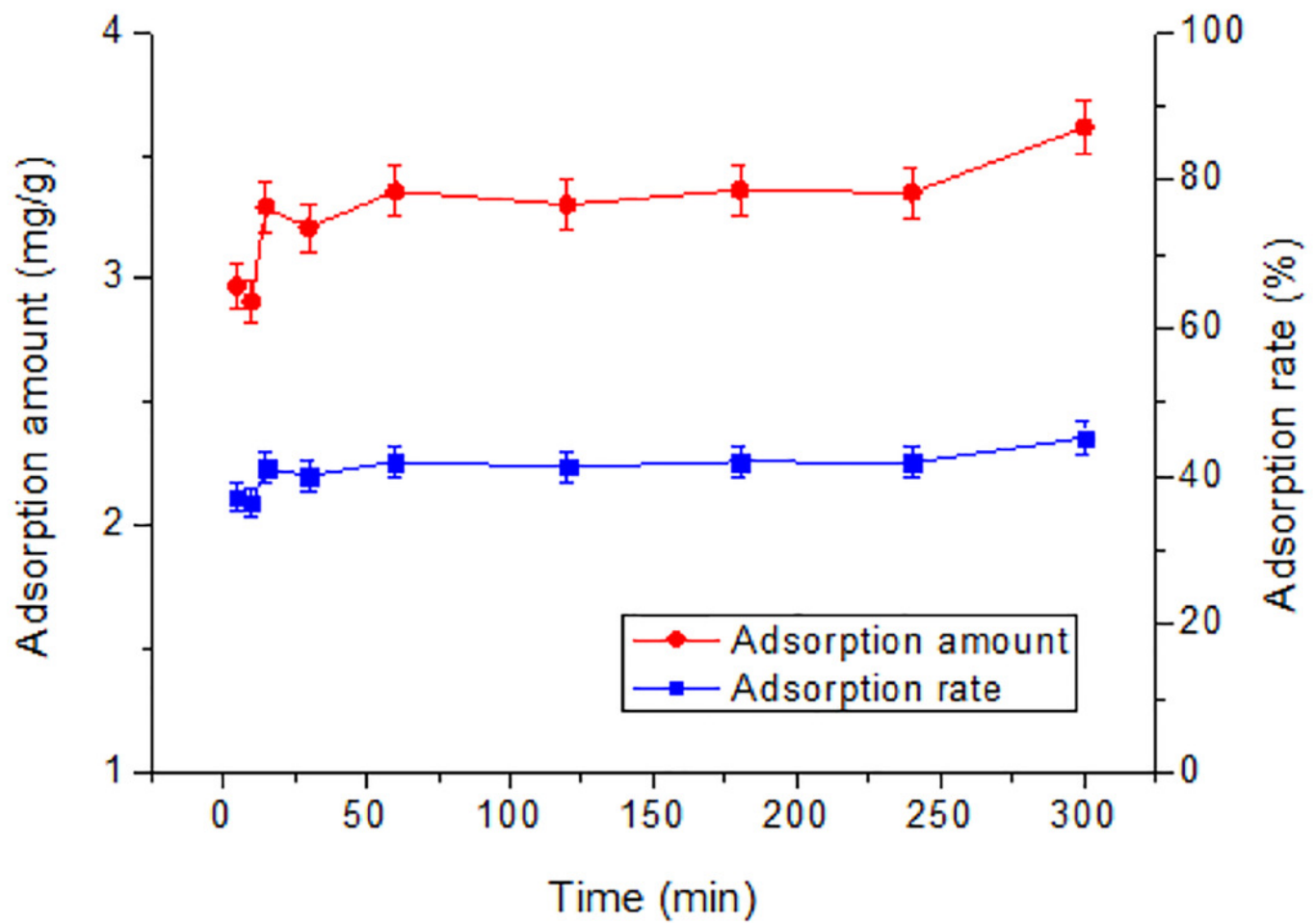
Figure 6

Adsorption isotherms of Tl on rutile nano-TiO$_2$
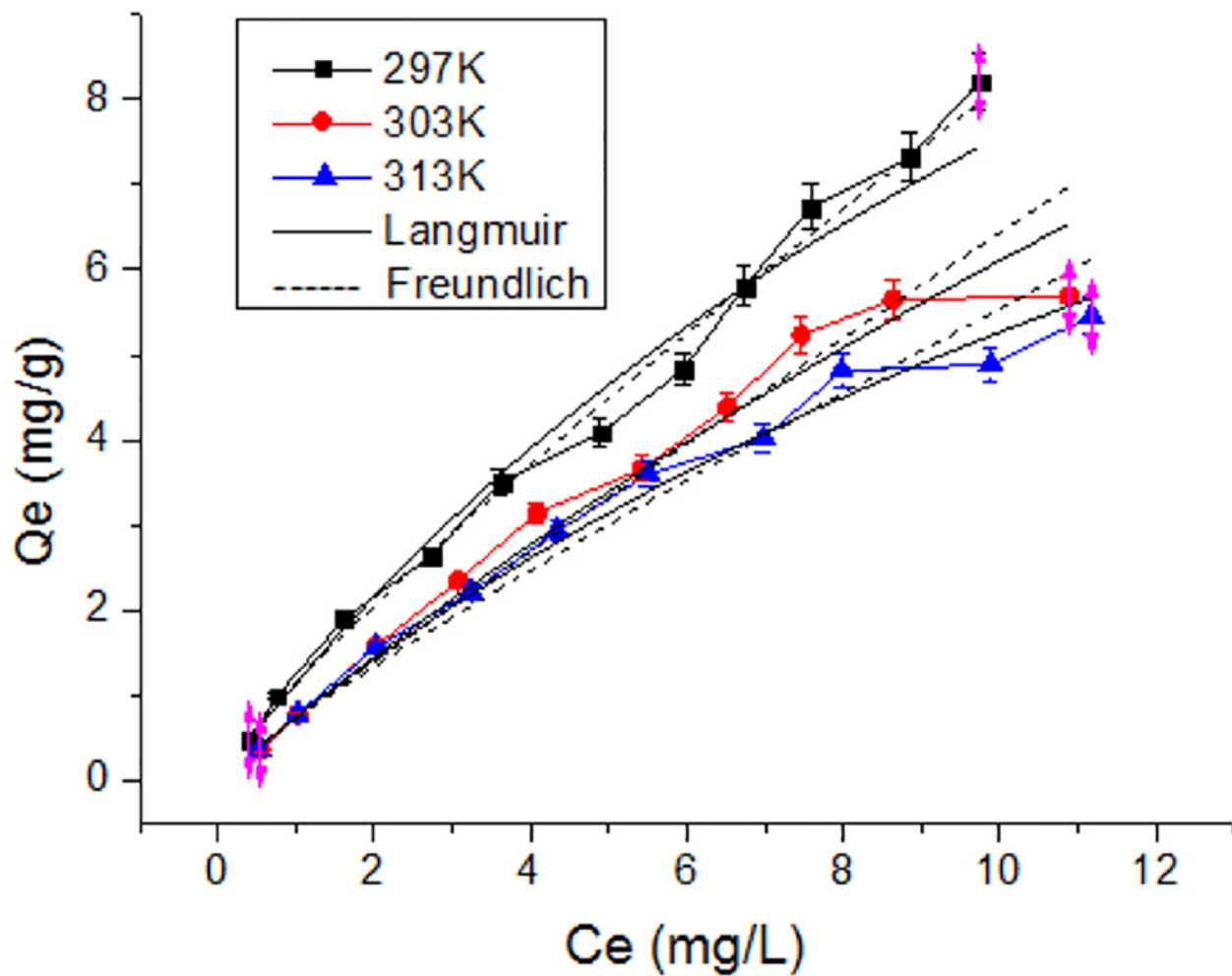
Figure 7

Infrared spectra of rutile nano-TiO$_2$
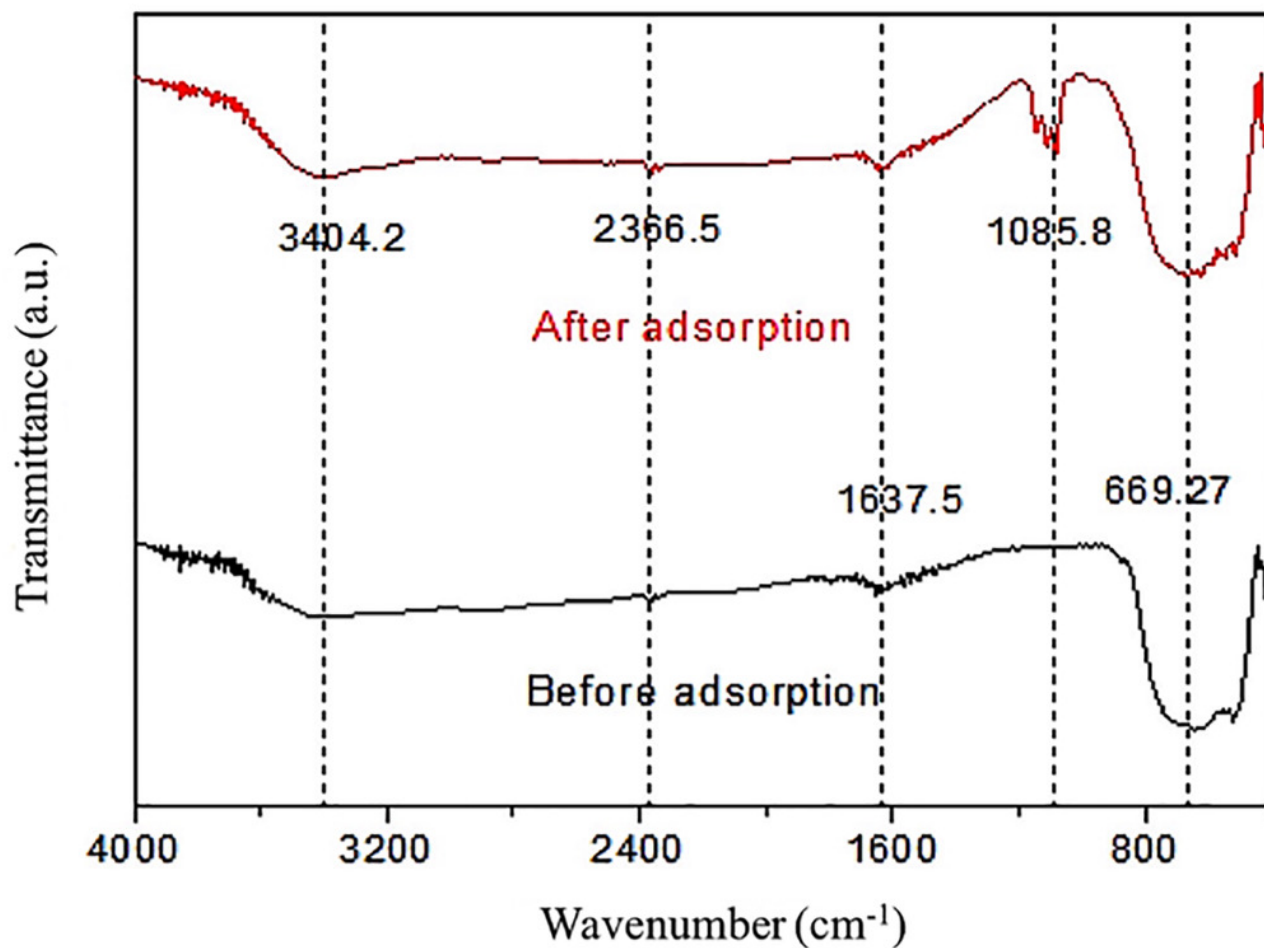
Figure 8

SEM-EDS image after adsorption of nano-TiO$_2$; (a) Before adsorption; (b) After adsorption
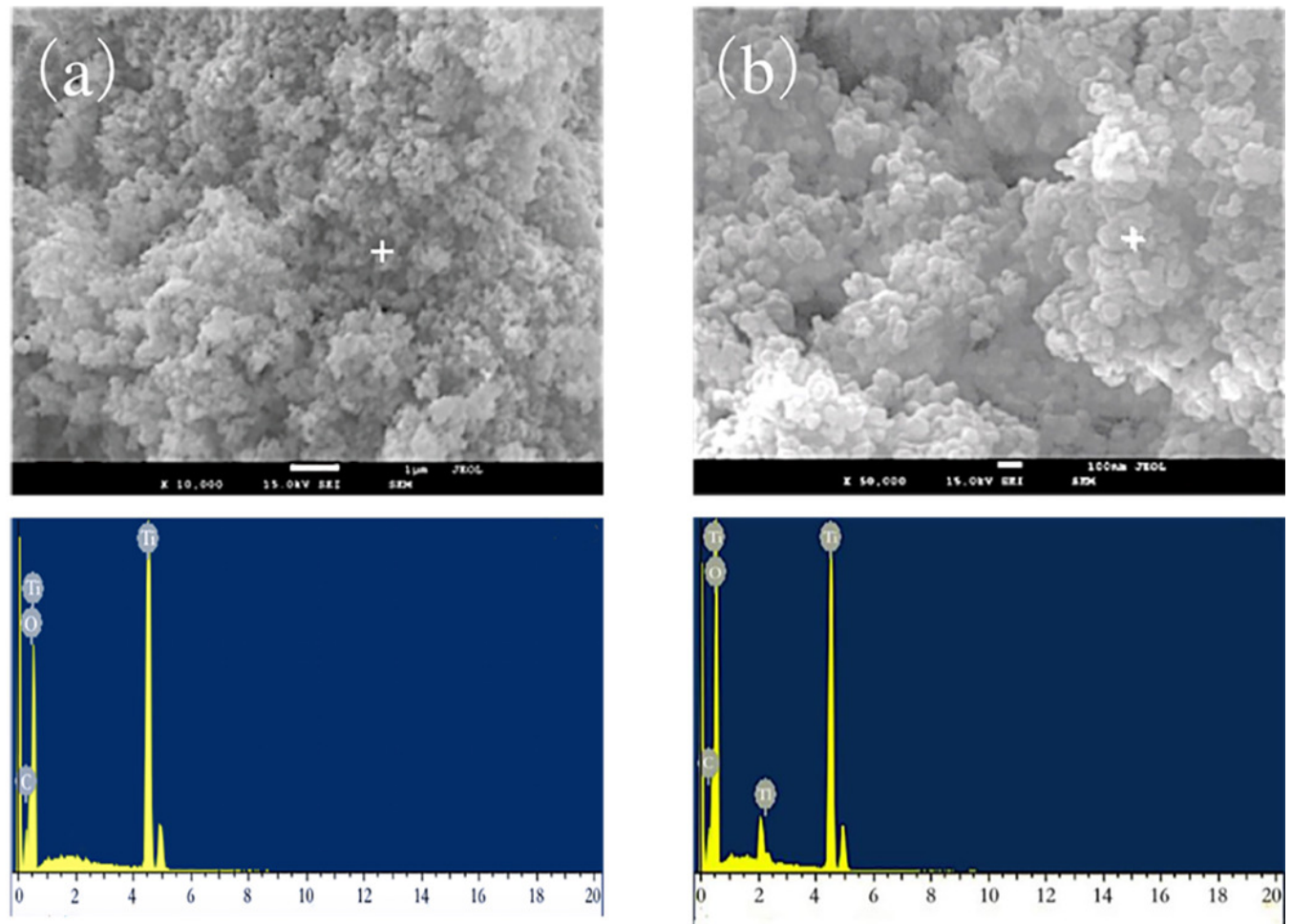
Figure 9

X-ray diffraction pattern of nano-TiO_2; (a) Before adsorption; (b) After adsorption
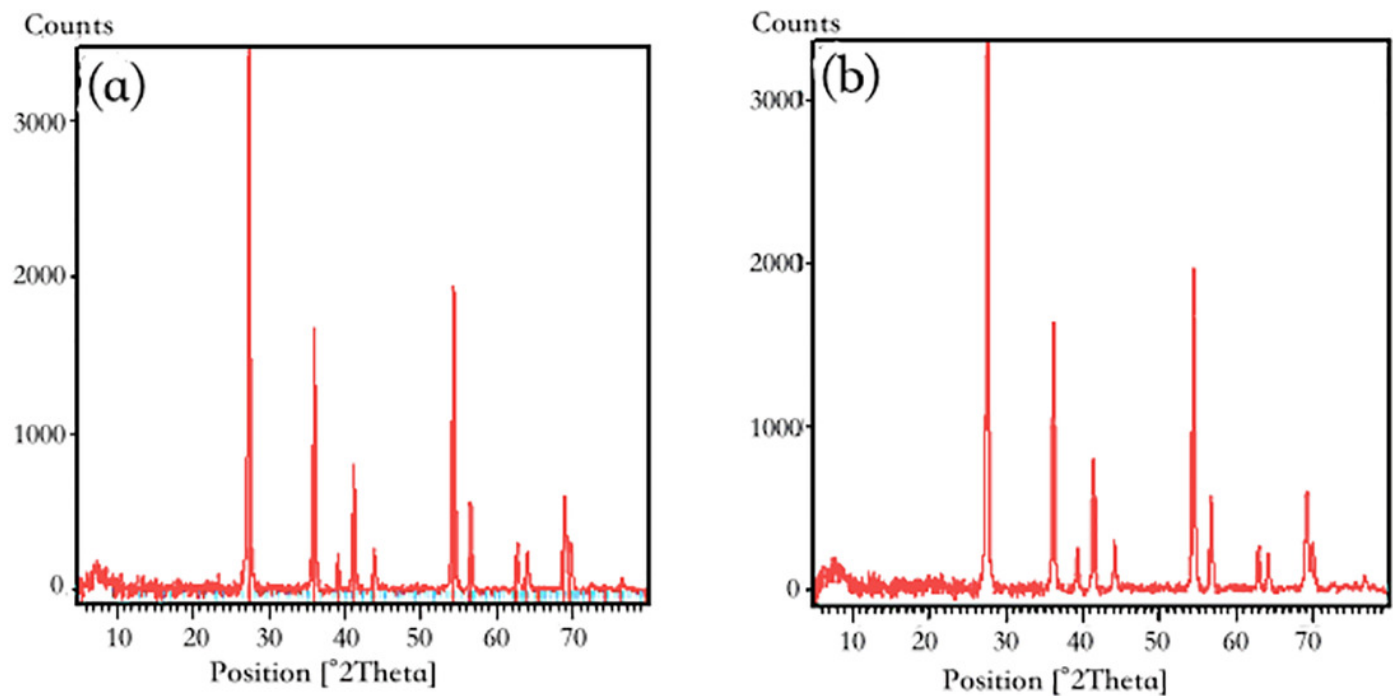
Kinetic parameters for adsorption of Tl(I) on rutile nano-TiO_2

1   Table. 1 Kinetic parameters for adsorption of Tl(I) on rutile nano-TiO_2

Quasi-first-order			Quasi-secondary			Elovich		
k_1	q_e	R^2	k_2	qe	R^2	k_e	C	R^2
0.0014	3.0285	0.6169	0.0857	3.5157	0.9969	0.1229	2.7796	0.6947

Isotherm parameters for adsorption of Tl(I) on rutile nano-TiO$_2$

1   Table. 2 Isotherm parameters for adsorption of Tl(I) on rutile nano-TiO$_2$

T/K	$\Delta H/(kJ \cdot mol^{-1})$	$\Delta S/(kJ \cdot mol^{-1}K^{-1})$	$\Delta G/(kJ \cdot mol^{-1})$
298	-2.19	-60.67	0.4567
303	-2.19	-60.67	-0.6763
313	-2.19	-60.67	-0.5992